Triggering and stabilizing oxygen redox chemistry in layered $LiNa_{1/3}Ru_{2/3}O_2$ enabled by stable Li-O-Na configuration

Xin Cao, Haifeng Li, Yu Qiao, Min Jia, Chao Li, Xiyan Yue, Pengfei Wang, Ping He, Jordi Cabana and Haoshen Zhou**

X. Cao, Dr. Y. Qiao, Dr. M. Jia, Prof. H. Zhou
Energy Technology Research Institute, National Institute of Advanced Industrial Science and Technology (AIST), 1-1-1, Umezono, Tsukuba 305-8568, Japan.

E-mail: yuqiao@xmu.edu.cn (Y. Q.); zhou88yu@yahoo.co.jp (H. Z.)

Dr. H. Li, Prof. J. Cabana

Department of Chemistry, University of Illinois at Chicago, Chicago, Illinois 60607, United States

Dr. P. Wang, Prof. P. He, Prof. H. Zhou

Center of Energy Storage Materials & Technology, College of Engineering and Applied Sciences, Jiangsu Key Laboratory of Artificial Functional Materials, National Laboratory of Solid State Microstructures, and Collaborative Innovation Center of Advanced Microstructures, Nanjing University, Nanjing 210093, P. R. China

E-mail: hszhou@nju.edu.cn (H. Z.)

X. Cao, Dr. M. Jia, Prof. H. Zhou

Graduate School of System and Information Engineering, University of Tsukuba, 1-1-1, Tennoudai, Tsukuba 305-8573, Japan

Dr. C. Li

Shanghai Key Laboratory of Magnetic Resonance, School of Physics and Electronic Science, East China Normal University, Shanghai 200062, P. R. China

Dr. X. Yue

Graduate School of Science and Technology, Hirosaki University, 1-Bunkyocho, Hirosaki 036-8560, Japan

Keywords: Li-O-Na configuration, cathode materials, layered oxides, oxygen redox reactions, long cycle life

Li-rich layered oxides are promising cathode candidates for high-energy-density Li-ion batteries due to their high output capacity triggered by both cationic and anionic redox reactions. However, the severe lattice oxygen loss inevitably induces the irreversible Li migration both in transition metal (TM) and Li layers, which deteriorates the stability of Li-O-Li configuration, further resulting in serious structural distortion and capacity decay. Herein, a stable Li-O-Na configuration was introduced within Li-based layered cathode material by Na substitution in TM layer, which not only triggers additional capacity based on oxygen redox reactions, but also introduces excellent structural and electrochemical stability upon cycling. By means of stable Li-O-Na configurations, the layered $Li[Na_{1/3}Ru_{2/3}]O_2$ exhibits reversible phase transition and structure evolution during Li^+ (de)intercalation processes, further boosting high output capacity (232 mAh g^{-1}) and long-term cycle stability (0.019 % per cycle after 1000 cycles). Comprehensive analysis of anionic/cationic redox reactions further clarifies the underlying charge compensation mechanisms. Altogether, these findings demonstrated that Na substitution can be regarded as an effective strategy to achieve stable oxygen redox chemistry within Li-based cathode materials.

1. Introduction

The family of Li-rich cathode materials, $xLi_2MnO_3 \cdot (1-x)LiMO_2$ (M = Mn, Ni, Co etc.), has attracted much attention as Li-ion battery cathodes because of their high specific capacity (exceeding 250 mAh g^{-1}) and compositional flexibility. In comparison to the commercial layered Ni-rich $LiNi_{1-x-y}Mn_xCo_yO_2$ $(x + y < 1)$, these Li-rich candidates further boost the energy density and lower the cost of manufacture for existing Li-ion battery systems. However, layered Li-rich oxide cathodes generally suffer from the serious oxygen release at high states of charge, which is caused by a detrimental oxidation of lattice O^{2-} ions to O_2 molecules upon charging. The lattice oxygen loss induces several issues. First, gaseous O_2 generated during charging process cannot be efficiently reduced back to lattice O^{2-} upon discharge, preventing the reversible migration of Li^+ ions back to the TM layer. It will accelerate the loss of Li-O-Li configuration, resulting in the serious capacity decay arising from the oxygen redox reactions. Furthermore, the oxygen loss and irreversible Li migration will exacerbate the irreversible TM migration from TM layer to Li layer. As a result, it causes the structural rearrangement, inducing the obvious layered to spinel phase transition, which leads to rapid decline of energy density upon initial several cycles.

Numerous efforts have been dedicated to addressing the issues of Li-rich cathode materials. Among them, surface/interface modifications, such as coatings, and tailoring of the composition in the TM layer, through doping and substitution strategies, are the most widely used, which yield improvements in structural and electrochemical stability in traditional Li-rich cathode materials. Besides, the strategies of novel structural design

and modification also effectively resolve the inherent problems of Li-rich cathode materials, which not only broadens the design ideas but also enriches the types of Li-rich materials. For instance, Eum et al. developed a novel Li-rich layered $Li_{0.83}[Li_{0.2}Ni_{0.2}Mn_{0.6}]O_2$ cathode by altering oxygen stacking arrangement to O2 rather than O3. The material displayed improved reversibility of the cation migration and excellent voltage retention upon cycling. Moreover, Cao et.al designed a O3-type layered $Li_{0.6}[Li_{0.2}Mn_{0.8}]O_2$ cathode material, where the Li deficiency in the Li layer and Li excess state in the TM layer combined to effectively restrain lattice oxygen release while reaching high oxygen-related capacity. However, most of these research works mainly focused on modifications that preserved Li-O-Li configuration in Li-rich cathode materials as a design target, in which the Li^+ ions within TM layer always irreversibly migrate to Li layer even to out of layered structure upon cycling. However, relatively stable oxygen redox behavior is also triggered in Na-based layered cathode materials via structural configurations different from Li-O-Li, which can be reached by various substitutions of vacancy, Li, Na, Mg, Zn, Cu etc. within the TM layers. Therefore, it is imperative to develop and enrich the significant configurations for Li-based cathode materials to realize stable cationic and anionic redox reactions.

In this work, Li-O-Na configurations were introduced in layered Li-based oxides for the first time, which not only trigger oxygen redox reactions to provide additional capacity but also stabilize the layered structure to achieve excellent cycling performances. This principle is exemplified with a novel layered oxide cathode $Li[Na_{1/3}Ru_{2/3}]O_2$ developed by chemical Li^+/Na^+ ion exchange strategy form

$Na[Na_{1/3}Ru_{2/3}]O_2$. $Li[Na_{1/3}Ru_{2/3}]O_2$ achieves a high discharge capacity of 232 mAh g^{-1} through a combination of anionic/cationic redox reactions. Benefiting from structural stability induced by Na substitution within TM layer, the electrode displays a reversible phase transition and structure evolution upon (de)lithiation processes, which underpins the electrochemical stability upon long-term cycling, resulting in the limited capacity loss of 0.021 % (per cycle upon 800 cycles) and 0.019 % (per cycle upon 1000 cycles) at current density of 50 and 200 mA/g. respectively. Besides, the existence of complex oxygen-related and Ru-based redox reactions is evaluated, which is beneficial for unravelling the charge compensation mechanisms of anionic and cationic chemistry.

2. Results and Discussion

2.1 Synthesis and Structural Characterization of $Na[Na_{1/3}Ru_{2/3}]O_2$ and $Li[Na_{1/3}Ru_{2/3}]O_2$

Layered $Li[Na_{1/3}Ru_{2/3}]O_2$ was prepared by chemical ion exchange from $Na[Na_{1/3}Ru_{2/3}]O_2$ (Na_2RuO_3) with disordered arrangement in TM layer. The Na-based precursor was synthetized by traditional solid-state reaction, which has been investigated in previous studies. The X-ray diffraction (XRD) pattern and Rietveld refinement results (Figure 1a and Table S1) proved that the Na-based precursor can be indexed as the space group of hexagonal $R\bar{3}m$ with layered structure. The calculated lattice parameters were a = b = 3.120(3) Å, c = 16.099(8) Å, V = 135.75 $Å^3$, α = β = 90° and γ = 120° with goodness-of-fitting parameters of R_{wp} (8.3 %) and χ^2 (3.19). Furthermore, the elemental analysis by inductively coupled plasma (ICP, Table S2)

confirmed the chemical formula as $Na[Na_{1/3}Ru_{2/3}]O_2$. In the XRD pattern $Na[Na_{1/3}Ru_{2/3}]O_2$, there is no absence of superlattice peaks in the range of diffraction angle from 20 to 30°, indicating the arrangement of Na and Ru is disordered within the TM layer. Therefore, $Na[Na_{1/3}Ru_{2/3}]O_2$ displays a typical O3-type layered structure with ABCABC oxygen stacking along the c-axis, in which Na^+ ions occupy prismatic sites in the alkali metal (AM) layer, and Na^+ and Ru^{4+} ions are located in octahedral sites within the TM layer (Figure 1a insert).

Scanning electron microscopy (SEM, Figure S1) revealed that the morphology of $Na[Na_{1/3}Ru_{2/3}]O_2$ particles is macrometric with irregular shape. Furthermore, transmission electron microscopy (TEM, Figure 1b) image clearly showed these microparticles consist of holey sheets with diameters of several hundred nanometers. In addition, selected area electron diffraction (SAED, Figure 1b insert) was collected for the (003) lattice plane, where the spacing is consistent with XRD result. High-resolution TEM (Figure 1c) revealed the interlayer spacing of about 0.53 nm, again consistent with the (003) plane. According to the magnified rectangle area (Figure 1c insert), it can be clearly observed the TM layer displayed disordered arrangement between Na and Ru atoms.

After chemical Li^+/Na^+ ion exchange in molten salts, Li^+ ions from substituted for original Na^+ ions in the AM layer of $Na[Na_{1/3}Ru_{2/3}]O_2$, whereas the composition and arrangement within TM layer was well preserved. It can be proved by the ICP result after ion exchange process since the ratios of Li, Na and Ru accord with the designed

chemical formula (Table S3), indicating the Na ions within TM layer can be still stored in the layered structure, and Na^+ ions in AM layer can be replaced by Li^+ ions. Moreover, the XRD pattern of as-prepared product presented the (003) main peak was located at around 18.03° (Figure 1d), demonstrating the only Li ions occupy the octahedral sites in the AM layer because the Na ions require larger interlayer distance to be located with the lower diffraction angle at around 16.59° (Figure 1a). The combination of XRD and ICP results forcefully demonstrated that Na^+ ions can be settled within TM layer, which achieves the introduction of Li-O-Na configuration in Li-based layered cathode material at the first time. According to the XRD Rietveld refinement results, the $Li[Na_{1/3}Ru_{2/3}]O_2$ could be indexed with the hexagonal space group of $R\bar{3}m$, corresponding to a lattice with an oxygen stacking arrangement of ABCABC (Table S4). The refined lattice parameters were a = b = 2.929(4) Å, c = 14.851(3) Å, V = 101.7 $Å^3$, $\alpha = \beta = 90°$ and $\gamma = 120°$, with satisfactory parameters, R_{wp} = 7.8 % and χ^2 = 2.67. Thus, the layered $Li[Na_{1/3}Ru_{2/3}]O_2$ have succeeded the disordering Na/Ru arrangement in TM layer form $Na[Na_{1/3}Ru_{2/3}]O_2$, in which all Li^+ ions was located in AM layers, delivering the Li-O-Na configuration along the c-axis direction (Figure 1d insert).

The morphology of $Li[Na_{1/3}Ru_{2/3}]O_2$ was also investigated with both SEM (Figure S2) and TEM (Figure 1e). The morphology of the powder was microparticulate with layered structure characteristics, again constructed by porous sheets at the nanometer scale. $Li[Na_{1/3}Ru_{2/3}]O_2$ exhibited the similar morphology with Na-based precursor, suggesting the chemical ion exchange strategy is a moderate method to harvest Li-based

layered materials with various structures. Both SAED (Figure 1e insert) and high-resolution TEM (Figure 1f) images detected an interlayer spacing of approximate 0.49 nm, which is consistent with the (003) plane, confirming Na^+ ions with larger radius have been replaced by Li^+ ions within the AM layer. Besides, the magnified rectangle area (Figure 1f insert) also provided direct evidence that the disorder in the TM layer can be also maintained after ion exchange, in agreement with the absence of superlattice peaks in the XRD pattern (Figure 1d).

2.2 Electrochemical performance of $Li[Na_{1/3}Ru_{2/3}]O_2$

The electrochemical performance of layered $Li[Na_{1/3}Ru_{2/3}]O_2$ as cathode material was investigated in Li half-cells using galvanostatic tests within the voltage range from 2.0 to 4.8 V at a current density of 50 mA/g (Figure 2a). The first charge profile exhibits a combination of a slope up to 4.5 V (vs Li/Li^+), followed by a high-voltage plateau at around 4.68 V, for an initial charge capacity of about 234 mAh g^{-1}. It might be attributed to combination of the Ru oxidation reaction and oxygen-centered redox reactions triggered by the Li-O-Na configuration, which would be unraveled in charge compensation mechanism section. During the subsequent discharge, the electrode delivered a capacity of 225 mAh g^{-1}, for a limited irreversible capacity of about 9 mAh g^{-1} during the initial cycle. Upon the second cycle, the charge and discharge curves exhibited the sloping profiles reminiscent of other Li-rich layered oxides with Li-O-Li configuration, such as $Li[Li_{0.2}Ni_{0.2}Mn_{0.6}]O_2$. Besides, the $Li[Na_{1/3}Ru_{2/3}]O_2$ electrode delivered a high output capacity of 232 mAh g^{-1} upon the second discharge, which is

close to the value of the charge capacity, suggesting the excellent coulombic efficiency and superior electrochemical reversibility can be achieved. Notably, excellent rate performance also can be realized in this cathode material (Figure 2b), as discharge capacities of 232, 215, 190, 163, 139 and 115 mAh g^{-1} were achieved at rates of 0.25, 0.5, 1, 2, 5, 10 C (1 C=200 mA/g), respectively. A high output capacity of 228 mAh g^{-1} also could be harvested again after the measurement of rate performance.

Limited capacity loss (0.021 % per cycle) and outstanding capacity retention (82.9 %) was obtained after 800 cycles at a low current density of 50 mA/g. In addition, the normalized 100th, 200th, 300th, 400th, 500th discharged curves displayed a stable output voltage (Figure S3), indicating the serious voltage decay in Li-rich cathodes with Li-O-Li configuration can be well restrained in $Li[Na_{1/3}Ru_{2/3}]O_2$ with Li-O-Na configuration. Moreover, even at high current density of 200 mA g^{-1}, the limited capacity loss (0.019 % per cycle upon 1000 cycles) and excellent capacity retention (81.1 % after 1000 cycles) also can be realized upon long cycling (Figure 2d). These electrochemical results indicate that stable electrochemical processes, favorable kinetics, and superior structural stability can be achieved in $Li[Na_{1/3}Ru_{2/3}]O_2$ with Li-O-Na configuration during long-term cycling.

2.3 Structural evolution within $Li[Na_{1/3}Ru_{2/3}]O_2$

Operando XRD was employed to investigate the processes of phase transition within a $Li[Na_{1/3}Ru_{2/3}]O_2$ electrode during delithiation/lithiation (Figure 3a and S4). According to both the contour plots and full-range XRD patterns, it can be clearly

observed that an obvious phase transition from the pristine O3 to an O1 structure occurred in the initial stage of the first charge. Such O1 structure subsquently dominated until the final stage of the first discharge, in which the (10-1) characteristic peak of O1 structure can be detected at around 40.8°. Notably, the reversible phase transition from O1- to O3-type layered structures appeared at the end of the first cycle, which displays a reversible structural evolution upon the first delithiation and lithiation process. Moreover, the shifts and transitions of (003)/(001), (006)/(002), (10-1) and (009)/(003) peaks also had a reversible process accompanied by the second Li^+ (de)intercalation process, which is similar with the evolutions during the first cycle, further demonstrating the reversible O1/O3 phase transition and structural evolution have been achieved upon the second cycles. The operando XRD results provided a solid foundation of the layered $Li[Na_{1/3}Ru_{2/3}]O_2$ electrode would harvest excellent reversibility of structural change during long-term cycling.

^{23}Na solid-state nuclear magnetic resonance (NMR) was also conducted to study the evolution of Na migration during Li^+ (de)intercalation processes (Figure 3b). For ^{23}Na solid-state NMR spectrum of Na-based layered $Na[Na_{1/3}Ru_{2/3}]O_2$, it exhibited two resonances at around 446 and 805 ppm at pristine state (Figure S5), which can be assigned as Li^+ ions located in AM layers (Na_{AM}) and TM layers (Na_{TM}), respectively. The ^{23}Na solid-state NMR spectrum of $Li[Na_{1/3}Ru_{2/3}]O_2$ electrodes collected at charged and discharged states, it can be deduced that Na^+ ions can be well preserved during cycling since the Na_{TM} signal can be detected with absence of the Na_{AM} signal. Besides, no-related layered Na-based phase can be observed within in-situ XRD patterns, further

demonstrating Na^+ ions would not migrate from TM layer to AM layer, which enhances the stability of Li-O-Na configuration upon charging and discharging processes. Altogether, the results of in-situ XRD and solid-state NMR demonstrated that the reversible phase transition and structural evolutions as well as stable Na substitution can be achieved within $Li[Na_{1/3}Ru_{2/3}]O_2$ electrode, which provides a solid foundation for excellent cycling performances at both low and high current density.

2.4 Analyses of redox reactions

The irreversible/reversible anionic oxygen redox behaviors within the layered $Li[Na_{1/3}Ru_{2/3}]O_2$ electrode were probed by the combination of mapping of resonant inelastic X-ray scattering (mRIXS) and in-situ differential electrochemical mass spectroscopy (DEMS) upon (de)lithiation processes. In comparison with the mRIXS collected at pristine state, the feature of oxidized lattice oxygen with low intensity can be observed at 531.5 eV excitation energy and 523.1 eV emission energy after the first charge process (Figure 4a and 4b), which is consistent with Ru/Ir-based cathode materials with anionic redox reactions. To further confirm the emergence of oxygen-related feature, the integrated RIXS spectra cut from the range of oxygen redox feature were shown at the pristine and the first charged states (Figure S6), which effectively demonstrated the oxygen oxidation reactions occurred upon the first charging process. Moreover, the mRIXS were also collected at the first discharge and second charged states (Figure S7), in which the feature of oxidized lattice oxygen was absent after discharged to 2.0 V and became distinct after recharged to 4.8 V, which is also

confirmed by the corresponding integrated RIXS spectra cut from the range of oxygen redox feature (Figure S8).

In-situ DEMS was employed within the layered $Li[Na_{1/3}Ru_{2/3}]O_2$ electrode to investigate the evolution of gaseous O_2 and CO_2 upon Li^+ (de)intercalation (Figure 4c). The CO_2 evolution can be divided into two regions. The first region started from 4.35 V generated by the oxidation reactions of carbonates such as Li_2CO_3, and the other region located at high voltage can be attributed to the nucleophilic attack on electrolyte caused by superoxo species and/or the decomposition of electrolyte at high voltage, in which the originations cannot be distinguished at our current experiment conditions. Moreover, O_2 evolution can be detected at 4.69 V, which only originates from the oxidization of lattice oxygen but cannot be assigned to carbonate oxidation nor electrolyte degradation. Therefore, according to the total amount of oxygen evolution (39.6 μmol/g), the irreversible capacity can be calculated as about 7.5 mAh/g based on the $4e^-$ reactions from $2O^{2-}$ to O_2. The results of mRIXS and DEMS indicated that not only can reversible oxygen redox reactions be well triggered within $Li[Na_{1/3}Ru_{2/3}]O_2$ electrode upon cycling, but also can the irreversible oxygen behaviors be well suppressed by means of Li-O-Na configuration.

To further study the evolution of the Ru oxidation state during cycling, Ru K-edge X-ray absorption spectroscopy (XAS) was conducted upon the initial two Li^+ de(intercalation) cycles (Figure 3d). The shifts of the rising edge can qualitatively reflect the evolution of Ru oxidation states during cycling (Figure 3d insert). Upon the first charge, the rising edge shifted toward higher energy relative to the pristine state,

demonstrating the Ru oxidation reaction was involved in the first Li removal process. after the subsequent discharge process, the rising edge shifted back to the original location, suggesting the Ru was reduced to original oxidation state after the first discharge. When recharged to 4.8 V, the rising edge shifted to slightly higher energy compared with the first charged state, suggesting the Ru was oxidized to a higher oxidation state in the second cycle. Fourier transform of the Ru K-edge was also performed to extract the extended X-ray absorption fine structure (EXAFS) and investigate the Ru local chemical environments (Figure S9). The locations of both Ru–O and Ru-Ru peaks have a relatively reversible evolution associated with Li^+ (de)intercalation, indicating the reversible structural evolutions can be realized in $Li[Na_{1/3}Ru_{2/3}]O_2$.

To further evaluate the capacity distributions of both Ru and O redox activities, the integral method was performed to gain the approximate Ru oxidation states within $Li[Na_{1/3}Ru_{2/3}]O_2$ electrode upon cycling. By applying the integral method, the linear relationship between Ru oxidation states and corresponding edge positions can be provided with regardless of spectra shapes (Figure 4e and 4f). In the first place, the hard Ru K-edge XAS spectra of RuO_2, Li_3RuO_4 and K_2RuO_4 were conducted to build a linear relationship between Ru oxidation states (+4, +5 and +6) and corresponding edge positions. Furthermore, the approximate Ru oxidation states within $Li[Na_{1/3}Ru_{2/3}]O_2$ electrode at different charged states can be roughly measured in the linear fit curve. The Ru valence was close to +4 at pristine state, which is well consistent with ICP results. Upon the initial cycle, the Ru was oxidized to +4.36 upon charging and further

reversibly reduced to +4.02 with neglect of a slight increase owning to the limitation of the accuracy of this technique. During the second charge, Ru had higher oxidation state (+4.45) than that at first charged state, in agreement with the analysis of hard Ru K-edge XAS results. More importantly, the capacity contributions of oxygen redox reactions upon cycling can be approximately by the difference between total electrochemical capacities and Ru-based capacities. Thus, the capacity distributions of Ru and O redox activities can be roughly summarized (Figure S10), suggesting both cationic and anionic redox reactions experienced a reversible process upon initial two cycles. In general, the combination of mRIXS, DEMS and hard Ru K-edge XAS has demonstrated that reversible Ru-based and O-centered redox reactions can be well achieved within $Li[Na_{1/3}Ru_{2/3}]O_2$ electrode by means of Li-O-Na configuration, which enhances the structural and electrochemical stability during long-term cycling.

3. Conclusion

In this study, linear Li-O-Na configurations were introduced in a Li-based layered cathode material, $Li[Na_{1/3}Ru_{2/3}]O_2$, using the TM composition and disordered arrangement of $Na[Na_{1/3}Ru_{2/3}]O_2$ as template in a chemical Li^+/Na^+ ion exchange process. Benefiting from the solid Na substitution within TM layer, the Li-O-Na configuration can be well maintained upon cycling, which enhances both structural and electrochemical stability during long-term cycling. As a result, not only can reversible oxygen redox reactions be triggered, but also can irreversible oxygen release be effectively restrained, in which a high output capacity of 232 mAh g^{-1} can be achieved

within layered $Li[Na_{1/3}Ru_{2/3}]O_2$ based on combination of reversible anionic/cationic redox reactions. Both reversible phase transition and structural evolution have been achieved upon (de)lithiation processes, which provides a solid foundation to realize the excellent electrochemical performances including voltage and capacity retentions upon long cycling. Our findings not only demonstrated that reversible anionic redox activities can be realized within Li-based cathode material by means of Li-O-Na configuration, but also provided a competitive structure for traditional Li-rich oxides with Li-O-Li configuration.

Supporting Information

Supporting Information is available from the Wiley Online Library or from the author.

Acknowledgements

X. C. and H. L. contributed equally to this work. J. C. and H. L. were supported by the National Science Foundation under Grant No. DMR-1809372. This research used resources of the Advanced Photon Source, a U.S. Department of Energy (DOE) Office of Science User Facility operated for the DOE Office of Science by Argonne National Laboratory under Contract No. DE-AC02-06CH11357. We thank Advanced Photon Source at Argonne National Laboratory. X. C. acknowledges the scholarship from the China Scholarship Council (CSC).

Received: ((will be filled in by the editorial staff))
Revised: ((will be filled in by the editorial staff))
Published online: ((will be filled in by the editorial staff))

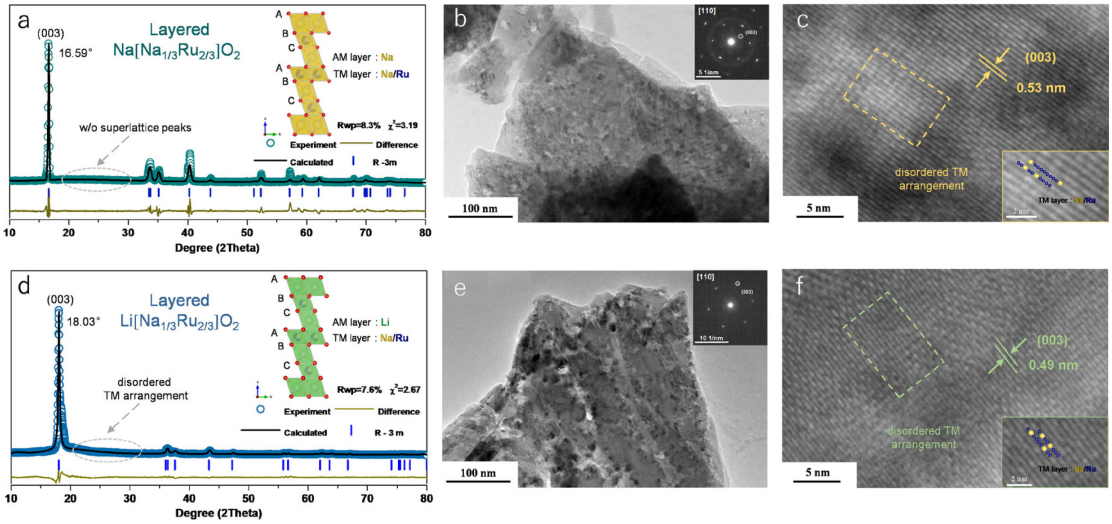

Figure 1. Structural characterization of layered $Na[Na_{1/3}Ru_{2/3}]O_2$ and $Li[Na_{1/3}Ru_{2/3}]O_2$. (a) XRD pattern of $Na[Na_{1/3}Ru_{2/3}]O_2$ and the corresponding results of Rietveld refinement. The X-ray target was Cu K_α with an incident wavelength of 1.54059 Å. The calculated pattern was obtianed by the software of General Structure Analysis System 2. The crystal structure of $Na[Na_{1/3}Ru_{2/3}]O_2$ viewed along the c-axis is depicted in the insert. (b) TEM and inserted SAED images of layered $Na[Na_{1/3}Ru_{2/3}]O_2$. (c) High-resolution TEM image of layered $Na[Na_{1/3}Ru_{2/3}]O_2$. (d) XRD pattern and Rietveld refinement results of $Li[Na_{1/3}Ru_{2/3}]O_2$ generated from $Na[Na_{1/3}Ru_{2/3}]O_2$ by Li^+/Na^+ ion exchange. (e) TEM and inserted SAED images of layered $Li[Na_{1/3}Ru_{2/3}]O_2$. (f) high-resolution TEM image of layered $Li[Na_{1/3}Ru_{2/3}]O_2$.

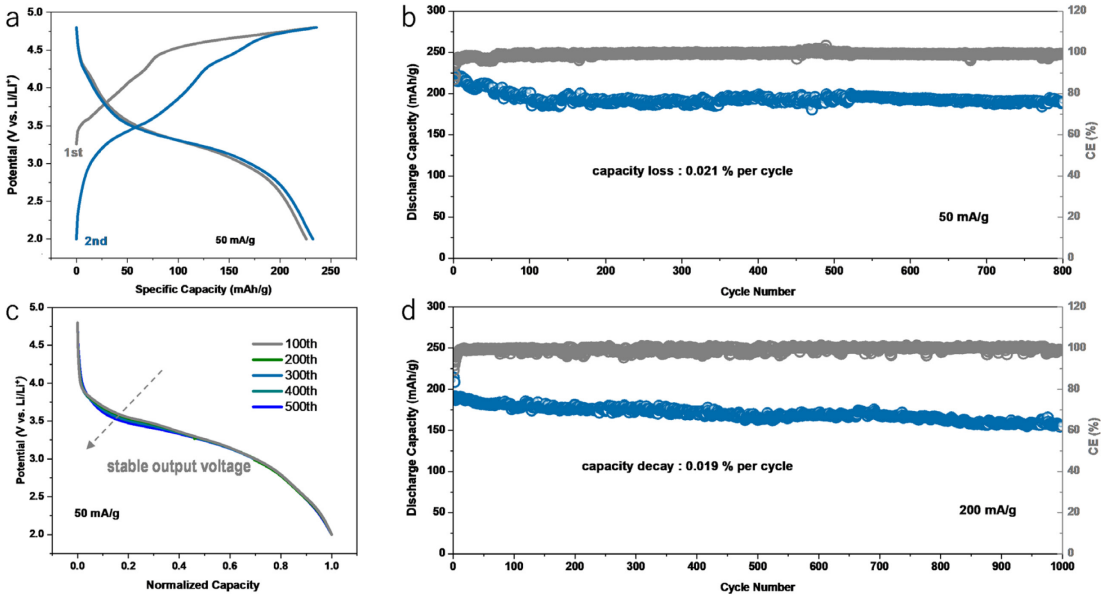

Figure 2. Electrochemical performance of $Li[Na_{1/3}Ru_{2/3}]O_2$. (a) Typical charge–discharge profiles of $Li[Na_{1/3}Ru_{2/3}]O_2$ during the first two cycles between 2 and 4.8 V. (b) Cycling performance of layered $Li[Na_{1/3}Ru_{2/3}]O_2$ between 2 and 4.8 V at a current density of 50 mA g^{-1}. (c) Normalized discharge profiles of $Li[Na_{1/3}Ru_{2/3}]O_2$ after 100, 200, 300, 400 and 500 cycles. (d) Capacity retention and coulombic efficiency (CE) of layered $Li[Na_{1/3}Ru_{2/3}]O_2$ between 2 and 4.8 V at a current density of 200 mA g^{-1}.

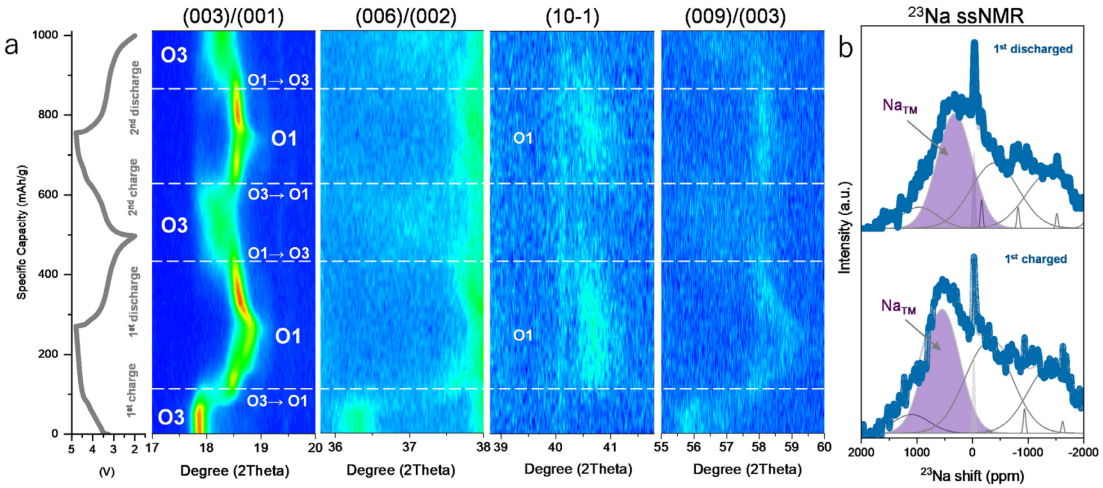

Figure 3. Phase transition and structural evolution of layered $Li[Na_{1/3}Ru_{2/3}]O_2$ upon cycling. (a) Contour plots of the (003), (006)/(002), (10-1) and (009)/(003) peaks of $Li[Na_{1/3}Ru_{2/3}]O_2$ derived from operando XRD experiments. (b) ^{23}Na solid state NMR spectra of the $Li[Na_{1/3}Ru_{2/3}]O_2$ electrode collected after the 1st charge and 1st discharge.

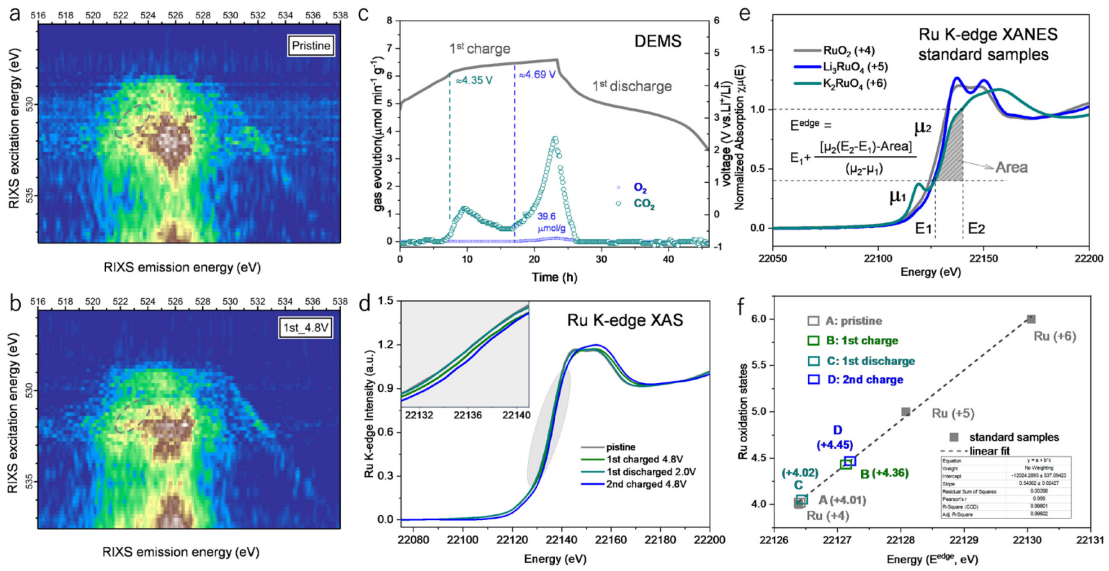

Figure 4. Analysis of anionic/cationic states in layered $Li[Na_{1/3}Ru_{2/3}]O_2$ upon cycling. O K-edge mRIXS of $Li[Na_{1/3}Ru_{2/3}]O_2$ electrode spectra obtained at (a) pristine and (b) 1st charged states. (c) Ru K-edge XAS of $Li[Na_{1/3}Ru_{2/3}]O_2$ at pristine, 1st charge, 1st discharge and 2nd charge states. (d) Operando differential electrochemical mass spectrometry (DEMS) of gas evolution during the first cycle. (e) Ru K-edge XAS of standard samples, RuO_2 (+4), Li_3RuO_4 (+5) and K_2RuO_4 (+6), for the evaluation of Ru oxidation states. (f) Linear relationship between the Ru oxidation states (+4, +5 and +6) and the K-edge positions determined by the integral method. The Ru oxidation states of $Li[Na_{1/3}Ru_{2/3}]O_2$ electrode at various charged states can be estimated by the linear relationship.